# Input-Output Constrained Adaptive Cruise Control

Panagiotis S. Trakas<sup>6</sup>, Valerio Modugno<sup>6</sup>, Dimitrios Kanoulas<sup>6</sup> and Charalampos P. Bechlioulis<sup>6</sup>

Abstract-In this paper, we introduce an adaptive cruise control (ACC) scheme that ensures collision avoidance by enforcing amplitude-and-rate constraints on the control input, while dynamically adapting output performance specifications. The proposed control strategy leverages the adaptive performance control (APC) methodology to handle asymmetrical input constraints, providing robust performance under diverse driving conditions. By incorporating multiple constraints into a unified funnel-based approach, the controller eliminates the need for complex optimization techniques, thereby maintaining low computational complexity. A rigorous theoretical analysis is provided, demonstrating the boundedness of all closed-loop signals and the overall feasibility of the control design. Comprehensive and comparative simulations highlight the ability of the proposed scheme to maintain a safe inter-vehicular distance, achieve accurate velocity tracking when state constraints allow and strict adherence to input limitations, resulting in improved passenger comfort. Finally, experimental validation using mobile robots confirms the effectiveness of the proposed ACC scheme in realworld conditions.

Index Terms—Cruise control, adaptive performance control, input constraints, autonomous driving

## I. INTRODUCTION

DAPTIVE Cruise Control (ACC) is an Advanced Driver-Assistance System (ADAS) [1] that automatically adjusts the speed of a vehicle, to maintain a safe following distance from the vehicle ahead. Unlike traditional cruise control, which maintains a constant speed, ACC uses sensors, such as cameras and radars, to monitor the distance and relative speed of preceding vehicles. By continuously processing this data, the ACC unit can dynamically adjust the vehicle's speed, decelerating when the leading vehicle slows down and accelerating when the road clears, without driver intervention ensuring compliance with state constraints. Thenceforward, state constraints within the control scheme guarantee a minimum following distance from the lead vehicle, imposing collision-free cruising.

This work was supported in part by the State Scholarships Foundation (IKY), the British Embassy in Athens, and the British Council in Greece under the Greek-British Collaboration for Short-Term Scholarships, in part by the Hellenic Foundation for Research and Innovation (H.F.R.I.) under the second call for research projects to support post-doctoral researchers (HFRI-PD19-370); and in part by the UKRI FLF [MR/V025333/1] (RoboHike). For the purpose of Open Access, the author has applied a CC BY public copyright license to any Author Accepted Manuscript version arising from this submission.

P. S. Trakas and C. P. Bechlioulis are with the Department of Electrical and Computer Engineering, University of Patras, Greece. V. Modugno and D. Kanoulas are with the RPL Lab, University College London, WC1E 6BT London, U.K. D. Kanoulas is also with the AI Centre, Department of Computer Science, University College London, Gower Street, WC1E 6BT, London, UK and Archimedes/Athena RC, Greece. E-mails: ptrakas@upatras.gr, v.modugno@ucl.ac.uk, d.kanoulas@ucl.ac.uk, chmpechl@upatras.gr.

ACC represents a significant step toward fully autonomous driving, as it automates a crucial aspect of vehicle operation, enhancing both safety and convenience. However, traditional ACC systems often face challenges in complex, real-world environments, and factors like sensor inaccuracies, actuator constraints, and rapidly changing traffic conditions can limit their effectiveness. These systems should balance the need to maintain a safe following distance while providing a smooth and efficient driving experience, as well as ensuring low computational complexity to facilitate real-time operation.

In the realm of traffic flow improvement, vehicle-following automation has been shown to offer substantial benefits over human drivers. The authors in [2], proposed a PID control law for automatic vehicle following, which ensures string stability, through a constant time headway rule, resulting in smoother traffic flow by mitigating the delays and errors inherent in human driving. In [3] the authors developed a PID controller that reduces the transient error and improves robustness. Moreover, the introduction of Cooperative Adaptive Cruise Control (CACC), which allows vehicles to communicate wirelessly with each other, has opened new avenues for traffic flow optimization. The work in [4] explored the impact of CACC on highway merging and stability, demonstrating improvements in traffic flow efficiency. The authors in [5] highlighted the need for more robust ACC algorithms that can be implemented in dynamic driving environments. The role of spacing policies in ACC has also garnered attention. In [6] various spacing policies were evaluated, concluding that a nonlinear spacing policy could offer superior traffic flow stability and capacity compared to the conventional time-gap controller. This insight reinforces the importance of carefully designed spacing policies to ensure both individual vehicle performance and broader traffic stability.

In terms of integrating collision avoidance and performance, advanced control techniques have been applied to ACC systems. A notable method that unifies Control Barrier Functions (CBFs) and Control Lyapunov Functions (CLFs) through quadratic programming was introduced in [7], [8]. This approach balances collision avoidance, represented by CBFs, with performance, represented by CLFs, while considering actuator limitations. The resulted scheme ensures that ACC systems can maintain desired speeds and safe following distances, while also adhering to acceleration and braking force constraints. Recently, the authors in [9] introduced the funnel cruise controller (FCC), a promising ACC approach ensuring that a safe following distance to the lead vehicle is never violated. While theoretically sound, the FCC does not account for practical input limitations, such as the force constraints imposed by the vehicle's engine, which can result in internal blow-up of the controller, leading to unbounded closed-loop

1

signals in real-world applications. Inspired by the FCC and building on our previous work on the adaptive performance control (APC) [10], [11], in this paper we aim at addressing the limitations of current ACC schemes by introducing a novel robust framework that rigorously incorporates input, output, and state (collision avoidance) constraints into the control strategy. The proposed approach guarantees adherence to state requirements, (i.e., maintaining a minimum following distance) and enforces hard input constraints, including maximum acceleration and jerk limits. Simultaneously, it dynamically adjusts the output performance specifications based on realtime input condition. By employing the APC technique, the proposed ACC system adapts to actuator limitations and sensor inaccuracies, ensuring robust performance across a wide range of driving scenarios. The key contributions of this work include:

- A novel ACC framework that guarantees state constraints and adaptive output performance by enforcing both amplitude and rate limitations on the control input, constraining both the vehicle's acceleration and jerk, unlike [9].
- A unified APC strategy that, unlike [10], [11], accommodates asymmetric saturation limits and performance boundaries relaxation.
- A robust control approach that integrates multiple constraints into a single funnel, eliminating the need for knowledge of model parameters or exploitation of approximation techniques.

The remainder of this paper is organized as follows. Section II formulates the multi-constrained control problem and presents some preliminaries on APC. In Section III-A, we design the input amplitude constrained ACC scheme, which integrates input-output and state constraints. Section III-B extends the design of Section III-A, to incorporate both amplitude and rate constraints. In Section IV, we present comprehensive and comparative simulation results, while Section V provides experimental validation using mobile robots to demonstrate the practical effectiveness of the proposed ACC framework. Finally, Section VI concludes the paper.

## II. PROBLEM STATEMENT AND PRELIMINARIES

Ground vehicles are composed of several key components, including the engine, transmission, wheels, brakes, etc. Although modeling the entire system can be highly complex, the model required for designing a cruise control system can be considerably simplified, as highlighted in [12]. The dynamics of the vehicle's motion is described by the following model:

$$\dot{x} = v$$

$$m\dot{v} = f_d(t, v) + u$$
(1)

where m (kg) is the total mass of the vehicle and x, v denote the position and velocity of the vehicle, respectively. Moreover, u (N) is the control input, representing the engine or braking force and  $f_d(t,v)$  is expressed as:

$$f_d(t,v) = -mgC_r\operatorname{sgn}(v) - \frac{1}{2}\varrho(t)C_dAv^2 - mg\sin\left(\theta(t)\right)$$

where  $g=9.81~(\text{m/s})^2$  is the gravitational acceleration,  $A~(\text{m}^2)$  is the frontal area of the vehicle, and  $C_r$ ,  $C_d$  are the rolling friction and aerodynamic drag coefficients, respectively. Additionally,  $\varrho(t)~(\text{kg/m}^3)$  denotes the time-varying but bounded air density, while  $\theta(t) \in [-\bar{\theta}, \bar{\theta}]$  (rad) represents the road slope, with  $\bar{\theta} \in <\frac{\pi}{2}$ . In this work, we focus on a scenario where a vehicle is following another, with  $x_p(t)$  and  $v_p(t)$  representing the position and velocity of the preceding vehicle, respectively.

## A. Control Objective

Let  $v_{\rm ref}(t)$  denote a smooth reference velocity, with unknown but bounded time derivative. The objective of this work is to design a state-feedback control scheme ensuring that the system (1) tracks the reference velocity  $v_{\rm ref}(t)$ , while strictly adhering to specific state and operational constraints. In particular, the proposed control scheme should guarantee that the closed-loop system satisfies the following constraints for all t > 0:

1) **State constraints (SC):** The inter-vehicular distance must satisfy the collision avoidance constraint:

$$d(t) := x_p(t) - x(t) > \delta \tag{SC}$$

with  $\delta$  representing a minimum safe distance when the vehicle is stationary.

2) Amplitude and rate input constraints (ARIC): A dynamic control law is formulated to satisfy both the amplitude and rate of change constraints on the control input:

$$\underline{u} = -c_d mg \le u(t) \le c_a mg = \bar{u}$$
 (AC)

$$\underline{r} \le \dot{u}(t) \le \bar{r}$$
 (RC)

where  $\underline{u} \in \mathbb{R}_{<0}$  and  $\bar{u} \in \mathbb{R}_{>0}$  denote the maximum allowable deceleration and acceleration forces, respectively. The parameters  $c_d$  and  $c_a$  represent user-defined factors of g, which can be adjusted based on the vehicle's specifications. Typically, a cruising experience involves limiting acceleration and deceleration forces to a range between -0.8g and 0.5g. Furthermore,  $\underline{r} \in \mathbb{R}_{<0}$  and  $\overline{r} \in \mathbb{R}_{>0}$  are constants that define the maximum allowable rate of change of the control input u(t), delimiting the jerk in the vehicle's motion.

3) Output performance constraints (OPC): The output tracking error e(t), to be formally defined later, is required to satisfy:

$$\rho^a(t) < e(t) < \rho^d(t) \tag{OPC}$$

where  $\rho^a(t)$  and  $\rho^d(t)$  are performance functions (PFs) that will be designed to dynamically adjust the soft constraints (OPC) when the hard constraints (AC),(RC) tend to be violated.

The performance specifications (OPC) ensure that the output tracking error is as small as possible, while maintaining compliance with the hard state (SC) and input (AC), (RC) constraints. To address the control problem outlined, we pose the following working assumptions:

**Assumption 1.** The relative position  $x(t) - x_p(t)$  between the controlled vehicle and the leading vehicle is assumed to be measurable using the vehicle's onboard sensors.

**Assumption 2.** The velocity of the leading vehicle,  $v_p(t)$  is unknown but bounded.

**Assumption 3.** The parameters in the system dynamics (1) are unknown. However, the total mass m of the vehicle and an upper bound on the absolute value of the road slope  $\bar{\theta} < \frac{\pi}{2}$  are assumed to be known.

Remark 1. In scenarios where input constraints are imposed, (i.e., both acceleration and jerk limits are applied to the system) it is necessary to assume knowledge of the nominal value for the mass of the vehicle (including passengers). The total mass can be estimated using the system's onboard sensors combined with a sensor fusion method, as proposed in [13]. The mass value is used to calculate the maximum accelerating and braking forces, defined as  $\bar{u} = c_a mg$  and  $u = -c_d mq$ , respectively. Furthermore, while this work does not rely on detailed information about the system parameters, it is important to note that the only term in  $f_d(\cdot)$  that can contribute to vehicle acceleration is the gravitational component  $mg\sin(\theta(t))$  when  $\theta \in [-\theta, 0)$ , (i.e., downhill driving). Given the hard constraints on both position and input, it is practical to assume that an absolute upper bound  $\theta$ on the road slope is known. This assumption facilitates a less conservative selection of the parameters  $c_d$  and  $c_a$ , as will be discussed in Section III-A1.

# B. Preliminaries on Adaptive Performance Control

APC is a control framework presented in [10] as an extension of prescribed performance control (PPC) [14], to ensure that a system adheres to output performance specifications despite uncertainties and input constraints. A key attribute of PPC-based approaches, is the normalized tracking error, which quantifies the deviation between the desired and actual system outputs, scaled by adaptive PFs that define the performance funnel over time. The normalized tracking error is defined as  $\xi_p(t):=\frac{e(t)}{\rho(t)},\; \rho(0)>|e(0)|,$  where e(t) is the tracking error and  $\rho(t)$  is the adaptive PF that imposes bounds of the acceptable performance funnel. The error transformation  $\epsilon_p(t) \coloneqq \ln\left(\frac{1+\xi(t)}{1-\xi(t)}\right)$  maps the constrained error dynamics into an unconstrained domain, with  $\epsilon:(-1,1)\to\mathbb{R}$ , facilitating the design of control laws that ensure predefined performance attributes. Additionally, the positive factor  $\zeta_p(t) :=$  $\frac{4}{\rho(t)(1-\xi(t)^2)}$  is used to scale the control signal in response to changes in the tracking error, enhancing the effectiveness of the control law to maintain desired system behavior. The control input is then given by  $u(t) := sat(u_d(t))$ , where  $u_d(t) := -k\zeta_p(t)\epsilon_p(t)$  and k > 0 is a control gain. The function  $sat(\cdot)$  is a saturation function that ensures the control signal remains within predefined bounds, thus respecting the input constraints.

To ensure the error remains strictly within the adaptive performance envelope in presence of hard input constraints, i.e.,  $-\rho(t) < e(t) < \rho(t)$ , the PF  $\rho(t)$  is dynamically adjusted through an adaptive law:

$$\dot{\rho} = -\lambda(\rho(t) - \rho^{\infty}) + \rho(t) \frac{u(t) - u_d(t)}{e(t)}$$

where  $\lambda$  is a positive constant regulating the convergence rate, and  $\rho^{\infty}$  represents the maximum allowable absolute steady-state error. Note that when e(t) is close to zero, it holds that  $u(t)-u_d(t)=sat(u_d(t))-u_d(t)=0$ , as saturation is not active in a neighborhood around e(t)=0. Consequently, the dynamics of  $\rho$  is well defined. The objective of APC is to design feedback control laws that ensure the tracking error evolves strictly within the adaptive performance envelope, allowing the controller to maintain bounded closed-loop signals and meet performance specifications, even when faced with conflicting input constraints.

## III. CONTROL DESIGN

In this section, we first design a robust ACC scheme that ensures compliance with the (SC), (AC) and (OPC) constraints. Then, we extend the design to incorporate both the amplitude and the rate constraints (RC), addressing the full input limitation scenario.

## A. Control Design under Amplitude Input Constraints

Generally, the force required to satisfy the hard state constraint (SC) conflicts with the input constraints (AC). To address this, we first introduce a time-varying safety distance function that guarantees the simultaneous satisfaction of both (SC) and (AC). Following this, we propose a static control law that ensures the closed-loop system adhere to the hard constraints (SC) and (AC), as well as the soft constraints (OPC).

1) Safety Distance: Inspired by [7] and considering the dynamics in (1), while neglecting the decelerating effects of rolling friction and aerodynamic drag, we obtain:

$$m\dot{v} = u - mg\sin\left(\theta(t)\right) \tag{2}$$

In the worst-case scenario, under maximum braking, the velocity of the vehicle after a time interval  $\tau$  can be determined by assuming the steepest negative slope,  $\theta(t+\tau)=-\bar{\theta}$ , which gives:

$$v(t+\tau) = v(t) - \tau g(c_d - \sin(\bar{\theta})). \tag{3}$$

Solving (3) for  $t_b$  seconds ahead, when the controlled vehicle stops, i.e.,  $v(t + t_b) = 0$ , we obtain:

$$t_b = \frac{v(t)}{q(c_d - \sin(\bar{\theta}))}. (4)$$

Note that  $c_d$  must be chosen such that  $c_d > \sin(\bar{\theta})$  for this condition to hold. Thus, the worst-case travelled distance  $x(t+t_b)$  after  $t_b$  seconds of maximum braking can be expressed as:

$$x(t+t_p) = x(t) + \int_{0}^{t_b} v(t+\tau)d\tau = x(t) + d_b(t)$$

with

$$d_b(t) = \frac{v(t)^2}{2g(c_d - \sin(\bar{\theta}))} \tag{5}$$

To address multiple hard constraints, including state and input limitations, we define a dynamically adaptive reference intervehicular distance as:

$$d_{\text{ref}}(t) := \delta + d_b(t) + \rho^{d,\infty}. \tag{6}$$

The proposed ACC framework is depicted in Fig. 1. To guarantee both collision avoidance and robust performance,  $d_{\text{ref}}(t)$  involves the following components:

- Minimum desired distance δ: Serves as a baseline to maintain safe spacing between vehicles when the velocity is zero.
- Time-varying safety distance  $d_b(t)$ : Calculated online based on (5), ensuring that the inter-vehicle distance never falls below the threshold  $\delta$ , even in scenarios involving maximum emergency braking.
- Prescribed performance parameters  $\rho^{a,\infty}$ ,  $\rho^{d,\infty}$ : Define the steady-state tracking performance set. These parameters regulate control accuracy, ensuring that the distance tracking error converges to zero when the intervehicle distance satisfies  $x(t) x_p(t) = \delta + d_b(t) + \rho^{d,\infty}$ .

The motivation for  $d_{\rm ref}(t)$  lies in its ability to incorporate both collision avoidance and performance constraints. When the vehicle enters the prescribed performance set  $(-\rho^{a,\infty},\rho^{d,\infty})$ , the controller prioritizes distance tracking to ensure safe cruising. This strategy guarantees collision-free operation while robustly imposing output performance specifications, related to both cruising speed and inter-vehicle distance, within actuation limitations.

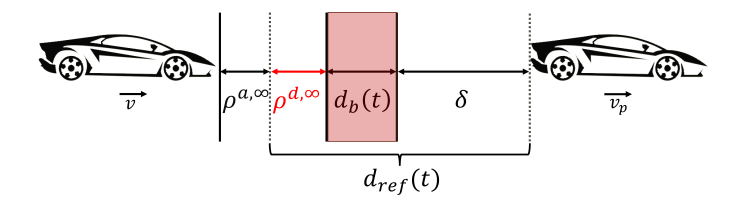


Fig. 1. Illustration of the proposed ACC framework. The highlighted area designate when the (AC) tend to be violated.

**Remark 2.** The safety distance  $d_b(t)$  is updated online, without incorporating the velocity of the leading vehicle or knowledge of the model parameters specified in (1), which may vary over time for both the controlled and leading vehicles. Consequently, the computed safety distance is conservative owing to the presence of hard input constraints, which conflicts with state constraints in emergency braking scenarios. Incorporating additional information would allow for an accurate estimation of the braking distances for both the lead and the controlled vehicles, as both the first and second terms in  $f_d(t, v)$  contribute to deceleration. This, in turn, would allow for a less conservative computation of  $d_b(t)$ . However, obtaining such information in real-time practical applications remains a significant challenge, and is left open for future research.

2) Static Control Law: Building on the APC methodology outlined in Section II-B we introduce the asymmetrical

adaptive PFs  $\rho^d(t)$  and  $\rho^a(t)$  (m/s), whose dynamics will be designed later in this section. The performance parameters  $\lambda^d>0$  and  $\lambda^a>0$  (s<sup>-1</sup>) regulate the exponential rate of tracking error convergence, while  $\rho^{a,\infty}>0$  and  $\rho^{d,\infty}>0$  (m) define the bounds of the residual set, within which the steady-state error evolves. Then, we define the asymmetric saturation function as:

$$\operatorname{sat}_{\underline{u}}^{\bar{u}}(u_d) \coloneqq \begin{cases} \bar{u} & \text{if} \quad u_d > \bar{u} \\ u_d & \text{if} \quad \underline{u} \leq u_d \leq \bar{u} \\ \underline{u} & \text{if} \quad u_d < \underline{u}. \end{cases}$$

and the tracking errors:

$$e_d(t) := \mu(x(t) - x_p(t) + d_{ref}(t))$$
 [Distance tracking error]  
 $e_v(t) := v(t) - v_{ref}(t)$  [Velocity tracking error].

To ensure consistency in units, a scaling factor  $\mu=1 {\rm s}^{-1}$  is introduced in the definition of  $e_d(t)$  allowing it to be expressed in m/s, similar to  $e_v(t)$ . In order to guarantee that the state constraint (SC) is always satisfied, while also ensuring that the velocity of the vehicle tracks the reference  $v_{\rm ref}(t)$  when (SC) is not violated, we define the output tracking error as:

$$e(t) := (1 - w(t))e_v(t) + c^w w(t)e_d(t) \tag{7}$$

where  $w(t) := \max\left(\frac{e_d(t) + \rho^a(t)}{\rho^d(t) - \rho^a(t)}, 0\right) \in [0, 1)$  with  $c^w > 0$  dictating the weight of the distance error  $e_d(t)$  on the output tracking error e(t). Note that w(t) < 1 as long as  $e_d(t) < \rho^d(t)$ . The switch function w(t) determines when the distance error  $e_d(t)$  begins to significantly affect the control strategy, thus enabling the transition from prioritizing velocity tracking to maintaining a safe following distance as the distance error increases. The normalized tracking error is defined as in [15]:

$$\xi(t) := \frac{e(t) - \frac{1}{2} \left( \rho^d(t) + \rho^a(t) \right)}{\frac{1}{2} \left( \rho^d(t) - \rho^a(t) \right)}.$$
 (8)

Next, we define the following control-related signals:  $\epsilon(t) \coloneqq \ln\left(\frac{1+\xi(t)}{1-\xi(t)}\right)$  and  $\zeta(t) \coloneqq \frac{4}{(\rho^d(t)-\rho^a(t))(1-\xi(t)^2)}$ . The constrained control input is then derived by:

$$u_d(t) := -k\zeta(t)\epsilon(t), \ k > 0$$
 (9)

$$u(t) := \operatorname{sat}_{u}^{\bar{u}}(u_d(t)). \tag{10}$$

The saturation function ensures that the control input u(t) remains within the predefined bounds  $[\underline{u}, \overline{u}]$ , ensuring the satisfaction of (AC). As shown in [9], a control input of the form  $u(t) = -ke_d(t)$ , with k > 0, can efficiently regulate the inter-vehicular distance for the system (1) in this context.

Finally, the adaptive performance laws that adjust the soft (OPC) constraints in response to the hard (AC) constraints are given by:

$$\dot{\rho}^d := -\lambda^d (\rho^d(t) - \mu \rho^{d,\infty}) + s_{\gamma^d}^e(t) \frac{u(t) - u_d(t)}{\xi(t) + 1} \tag{11}$$

$$\dot{\rho}^a := -\lambda^a (\rho^a(t) + \mu \rho^{a,\infty}) + s_{\gamma^a}^{-e}(t) \frac{u(t) - u_d(t)}{1 - \xi(t)}$$
 (12)

where the initial condition is set such that  $\rho^a(0) < e(0) < \rho^d(0)$ . Subsequently, the switch function  $s_a^b(\cdot)$  (1/kg) is defined as:

$$s_a^b(t) := \begin{cases} a, & b(t) \ge 0\\ 0, & b(t) < 0. \end{cases}$$
 (13)

Additionally,  $\gamma^d$  and  $\gamma^a$  are positive constants scaling the second term in (11) and (12), respectively.

**Theorem 1.** Consider the system described by (1), a smooth reference velocity  $v_{ref}(t)$  and a leading vehicle obeying Assumptions 1-3. The proposed amplitude constrained adaptive cruise controller (AC-ACC) (6)-(12) guarantees that the velocity tracking error remains within the adaptive performance bounds:

$$\frac{\rho^{a}(t) - c^{w}w(t)e_{d}(t)}{1 - w(t)} < v(t) - v_{ref}(t) < \frac{\rho^{d}(t) - c^{w}w(t)e_{d}(t)}{1 - w(t)}$$
(14)

while ensuring that: (i) the closed-loop signals  $x(t), v(t), u_d(t), \rho^a(t)$  and  $\rho^d(t)$  remain bounded, and (ii) the constraints (SC), (AC) and (OPC) are satisfied for all t > 0.

*Proof.* See the Appendix.

**Remark 3.** Note that  $\rho^d(t) \geq \mu \rho^{d,\infty} > 0$  and  $\rho^a(t) \leq$  $-\mu\rho^{a,\infty}$  < 0 for all  $t \geq 0$ . Hence, when e(t) > 0, the second term in (11) is activated by the function  $s_{\gamma d}^{e}(t)$  and increases  $\rho^d(t)$ . Conversely, when e(t) < 0, the second term in (12) is activated by the function  $s_{\sim d}^{-e}(t)$  and decreases  $\rho^a(t)$ . Thus, the performance adaptations are mutually exclusive; only one function is active at a time, based on the sign of e(t). The performance funnel, defined by  $\rho^{d}(t)$  and  $\rho^{a}(t)$ , is dynamically adapted in response to input saturation to maintain bounded signals in the closed-loop system. When the control input is not saturated, the PFs return to their predefined form, converging to  $\rho^{i,\infty}$  with a rate no less than  $\lambda^i$  for  $i = \{d, a\}$ , thereby ensuring that the tracking error is as small as possible, within the limitations imposed by the hard (AC) constraints. Further details on the selection of parameters  $k, \lambda^i, \rho^{i,\infty}, \gamma^i, i \in \{d, a\}$  are provided in Remark 4 of [16].

**Remark 4.** The tracking error e(t) adheres to the (OPC) constraints, as it is guaranteed that  $\rho^a(t) < e(t) < \rho^d(t)$ for all  $t \geq 0$ . This ensures that e(t) converges exponentially to the residual set  $(-\mu\rho^{a,\infty},\mu\rho^{d,\infty})$  when input saturation is inactive. However, when input saturation occurs, the performance specifications are relaxed in response to the system's input limitations. During this period, the vehicle either accelerates at its maximum capacity or decelerates under maximum braking. In the case of maximum acceleration, the PF  $\rho^a(t)$ decreases, loosening the output constraints to allow the vehicle to track the reference velocity as soon as possible. On the other hand, as shown in (5), under maximum braking, in the worst case scenario the inter-vehicular distance is reduced by  $d_b(t)$  until  $v(t) \to 0$ . Hence, based on (6), the minimum inter-vehicular distance under maximum braking is  $d(t) > \delta$ , thereby satisfying (SC).

B. Control Design under Amplitude and Rate Input Constraints

Limiting jerk, i.e., the rate of change of acceleration, is crucial for maintaining passenger comfort by avoiding abrupt, uncomfortable movements during acceleration or braking. It also enhances vehicle stability by preventing sudden shifts in weight distribution, which can degrade control efficiency, especially in emergency situations or on slippery surfaces. Furthermore, regulating jerk reduces mechanical wear on the vehicle's suspension and braking system, ensuring smoother and safer driving performance.

In this subsection, we extend the approach outlined in Section III-A, proposing a dynamic control law that ensures compliance with the hard rate input constraints (RC) as well. The design procedure for the dynamic adaptive cruise controller is organized into two main steps. First, we introduce a time-varying safety distance function to cope with control amplitude and slew-rate constraints and then we formulate the control signal to meet both output specifications and input constraints with respect to the amplitude of the control signal. Subsequently, building on our previous work [11], we develop the dynamic control law to simultaneously address the hard amplitude (AC) and rate (RC) input constraints and the soft output constraints (OPC).

# **Step 1: Design the signal incorporating** (AC)

- i Select the positive output performance parameters  $\lambda_o^d$  (s<sup>-1</sup>) and  $\lambda_o^a$  (s<sup>-1</sup>),  $\rho_o^{a,\infty}$  (m) and  $\rho_o^{d,\infty}$  (m) as described in Section III-A2.
- ii Select the safety distance:

$$d_{b,r}(t) := \frac{v(t)^2}{2g(c_d - \sin(\bar{\theta}))} + v(t)t_r + \frac{(u(t) + mg\sin(\bar{\theta}))t_r^2}{2m}$$

$$(15)$$

with  $t_r = \frac{u(t) + c_d mg}{|\underline{r}|}$ . Further details on the derivation of (15) can be found in the analysis between (50)-(54) in the Appendix. Additionally, select the reference distance:

$$d_{\text{ref}}^r(t) := \delta + d_{b,r}(t) + \rho_o^{d,\infty}.$$
 (16)

Define the distance error  $e_d(t) \coloneqq \mu(x(t) - x_p(t) + d_{\mathrm{ref}}^r(t))$  as well as the velocity error  $e_v(t) \coloneqq v(t) - v_{\mathrm{ref}}(t)$ . The parameter  $\mu = 1 \ (\mathrm{s}^{-1})$  ensures unit consistency as in Section III-A2. Hence, the output tracking error is similar to (7):

$$e_o(t) := (1 - w_o(t))e_v(t) + c_o^w w_o(t)e_d(t)$$
 (17)

where  $w_o(t) := \max\left(\frac{e_d(t) + \rho_o^a(t)}{\rho_o^d(t) - \rho_o^a(t)}, 0\right) \in [0, 1)$ , with  $c_o^w > 0$ .

iii Next define:

$$\xi_o(t) := \frac{e_o(t) - \frac{1}{2} \left( \rho_o^d(t) + \rho_o^a(t) \right)}{\frac{1}{2} \left( \rho_o^d(t) - \rho_o^a(t) \right)} \tag{18}$$

where  $\rho_o^d(t)$  (m/s) and  $\rho_o^a(t)$  (m/s) represent the adaptive PFs to be designed. Additionally, define the signals  $\epsilon_o(t) \coloneqq \ln\left(\frac{1+\xi_o(t)}{1-\xi_o(t)}\right)$  and  $\zeta_o(t) \coloneqq \frac{4}{(\rho_o^d(t)-\rho_o^a(t))(1-\xi_o(t)^2)}$ .

iv Introduce the following control-related signals:

$$u_d(t) := -k_o \zeta_o(t) \epsilon_o(t), \ k_o > 0 \tag{19}$$

$$u_s(t) \coloneqq \operatorname{sat}_u^{\bar{u}}(u_d).$$
 (20)

v The output performance constraints are governed by the following adaptive laws:

$$\dot{\rho}_o^d := -\lambda_o^d(\rho_o^d(t) - \mu \rho_o^{d,\infty}) + s_{\gamma_o^d}^e(t) \frac{u_s(t) - u_d(t)}{\xi_o(t) + 1} \tag{21}$$

$$\dot{\rho}_o^a := -\lambda_o^a(\rho_o^a(t) + \mu \rho_o^{a,\infty}) + s_{\gamma_o^a}^{-e}(t) \frac{u_s(t) - u_d(t)}{1 - \xi_o(t)} \tag{22}$$

with  $s_a^b(\cdot)$  (kg<sup>-1</sup>) denoting the switch function (13).

# Step 2: Design the signal incorporating (RC)

i Define the control input tracking error as:

$$e_u(t) \coloneqq u(t) - u_s(t) \tag{23}$$

where u is the actual control input and  $u_s$  is the amplitude saturated control signal.

- ii Select the positive input performance parameters  $\lambda_u^d$  and  $\lambda_u^a$  (s<sup>-1</sup>),  $\rho_u^{a,\infty}$  (N) and  $\rho_u^{d,\infty}$  (N) as described in Section III-A2
- iii Define the normalized input tracking error:

$$\xi_u(t) := \frac{e_u(t) - \frac{1}{2} \left( \rho_u^d(t) + \rho_u^a(t) \right)}{\frac{1}{2} \left( \rho_u^d(t) - \rho_u^a(t) \right)} \tag{24}$$

where  $\rho_u^d(t)$  (N) and  $\rho_u^a(t)$  (N) denote the adaptive PFs to be designed. Additionally, define the signals  $\epsilon_u(t) \coloneqq \ln\left(\frac{1+\xi_u(t)}{1-\xi_u(t)}\right)$  and  $\zeta_u(t) \coloneqq \frac{4}{(\rho_u^d(t)-\rho_u^a(t))(1-\xi_u(t)^2)}$ . iv Define the signal  $u_r(t)$  (N/s) related to the rate of change

iv Define the signal  $u_r(t)$  (N/s) related to the rate of change of the control input as:

$$u_r(t) := -k_u \zeta_u(t) \epsilon_u(t), \ k_u > 0. \tag{25}$$

v The control input is then governed by the following law:

$$\dot{u} := \operatorname{sat}_r^{\bar{r}}(u_r(t)), \ u(0) \in [\underline{u}, \bar{u}]$$
 (26)

where the saturation function ensures that the time derivative of the control input remains within predefined bounds  $[r, \bar{r}]$ .

vi The performance constraints of  $e_u(t)$  are governed by the following adaptive laws:

$$\dot{\rho}_u^d := -\lambda_u^d (\rho_u^d(t) - \rho_u^{d,\infty}) + s_{\gamma_u^d}^e(t) \frac{\operatorname{sat}_{\underline{r}}^{\bar{r}}(u_r(t)) - u_r(t)}{\xi_u(t) + 1}$$
(27)

$$\dot{\rho}_u^a := -\lambda_u^a (\rho_u^a(t) + \rho_u^{a,\infty}) + s_{\gamma_u^a}^{-e}(t) \frac{\operatorname{sat}_r^{\bar{r}}(u_r(t)) - u_r(t)}{1 - \xi_u(t)}$$
(28)

with  $s_a^b(\cdot)$  denoting a switch function given by (13).

**Corollary 1.** Under the conditions of Theorem 1, there exists  $\lambda_u^* > 0$  such that for all  $\lambda_u^d > \lambda_u^*$ , the proposed amplitude-and-rate constrained adaptive cruise controller (ARC-ACC) (16)-(28), guarantees that the velocity tracking error remains within the adaptive performance bounds (14), while ensuring that: (i) the closed-loop signals  $x(t), v(t), u_d(t), \rho_o^a(t), \rho_o^d(t), \rho_o^h(t), \rho_o^h(t)$  and  $u_r(t)$  remain

bounded, and (ii) the constraints (SC), (AC), (RC) and (OPC) are satisfied for all  $t \ge 0$ .

*Proof.* See the Appendix. 
$$\Box$$

Remark 5. The output performance of the closed-loop system is governed by the evolution of the PFs  $\rho_0^d(t)$  and  $\rho_0^a(t)$ . When the signal  $u_d(t)$  reaches saturation, these performance constraints need to be relaxed to ensure the boundedness of the closed-loop signals. The extent of this relaxation is influenced by the controller gains  $k_o$ ,  $\gamma_o^d$ ,  $\gamma_o^a$  and the convergence rates  $\lambda_o^d$  and  $\lambda_o^a$ . Additionally, the relaxation is affected by the control input tracking error  $e_u(t)$  [11], which should be maintained low. To achieve faster convergence of  $e_u(t)$ , higher values for the parameters  $k_u$ ,  $\lambda_u^d$  and  $\lambda_u^a$  are advantageous. However, selecting large values for the gains  $k_i$ ,  $i = \{o, u\}$ , may lead to excessive relaxation of the PFs (21)-(22) and (27)-(28), potentially causing unnecessary degradation of tracking accuracy. This is because larger gains can cause the signals  $u_d(t)$  and  $u_r(t)$  to reach saturation faster, increasing the second term in the corresponding adaptive performance laws, which may result in overshoot and slower convergence. Therefore, gain tuning must strike a balance between achieving rapid tracking error convergence and preserving the prescribed performance specifications, minimizing any unnecessary performance degradation.

**Remark 6.** The proposed control design is developed for a dynamical model (1) where u represents the force input, incorporating both engine propulsion and braking forces. Notably, the proposed control protocol can be readily implemented in a kinematic vehicle model of the form:

$$\dot{x} = u \tag{29}$$

where u (m/s) is now the velocity control input, subject to constraints  $u \in [u, \bar{u}]$  with its rate of change (acceleration)  $\dot{u} \in [r, \bar{r}]$ . The transition from the dynamical to the kinematic framework is justified under the assumption that the velocity control input u is directly available, which is a reasonable simplification in many robotic and autonomous vehicle applications. In practice, this assumption holds when a low-level controller ensures accurate tracking of velocity commands with negligible error. Regarding collision avoidance guarantees, the safety distance  $d_{b,r}(t)$  in the dynamical model case accounts for acceleration and jerk constraints. In the kinematic model framework, the safety distance  $d_{b,r}(t)$  captures the maximum distance required until the velocity command u reaches zero while respecting acceleration constraints. After straightforward algebraic manipulations, the simplified safety distance is given by:

$$d_{b,r}(t) := v(t)t_r + \frac{u(t)t_r^2}{2} \tag{30}$$

where v(t) denotes the velocity of the vehicle, with  $t_r = \frac{u(t)}{|r|}$ . Notably, at the kinematic level, neither the vehicle mass nor an upper bound on the road slope is required to be known. Thus, the proposed (ARC-ACC) (16)-(28) controller remains applicable across both dynamical and kinematic frameworks.

## IV. SIMULATION RESULTS

The proposed AC-ACC and ARC-ACC schemes were implemented and tested across two distinct driving scenarios to validate their effectiveness and demonstrate their efficacy compared to the FCC, presented in [9]. Both scenarios were simulated in MATLAB using the ode15s solver with relative and absolute error tolerances set to RelTol =  $10^{-10}$  and AbsTol =  $10^{-10}$ , respectively. The model and control parameters remained unaltered throughout the simulations and are summarized in Table I.

TABLE I SIMULATION PARAMETERS

Model Parameters	Controller Parameters		
$m=1100~\mathrm{kg}$	$k_o = 45 \text{ kg} \cdot \text{m}^2/\text{s}^3$	$c_o^w = 1$	$\rho_u^{d,\infty} = 10 \text{ N}$
$\theta = -0.1 \text{ rad}$	$k_u = 500 \text{ N}^2/\text{s}$	$\lambda_o^d = 2 \frac{1}{8}$	$\rho_u^{a,\infty} = 10 \text{ N}$
$C_r = 0.01$	$\bar{r} = 3000 \frac{N}{s}$	$\lambda_o^a = 0.5 \frac{1}{s}$	$\gamma_o^d = 1$
$C_d = 0.32$	$\underline{r} = -4000 \frac{N}{s}$	$\lambda_u^{d/a} = 10^{\circ} \frac{1}{\text{s}}$	$\gamma_o^a = 1$
$\varrho(t)=1.3~{ m kg/m^3}$	$c_d = 1.1$	$\rho_o^{d,\infty} = 0.5 \text{ m}$	$\gamma_u^d = 1$
$A = 2.4 \text{ m}^2$	$c_a = 0.9$	$\rho_o^{a,\infty}=0.2~\mathrm{m}$	$\gamma_u^a = 1$

## A. Generic Evaluation

In this simulation scenario, we demonstrate the effectiveness of the ARC-ACC (16)-(28) in maintaining both state and adaptive performance under amplitude-and-rate input constraints. Initially, the lead vehicle cruises at a constant speed 20~m/s for 80 seconds. Subsequently, the lead vehicle's speed oscillates according to  $\cos(0.25t)$ , simulating fluctuating traffic conditions. The ACC scheme was tasked with maintaining a minimum inter-vehicular distance  $\delta=2~m$  while tracking a reference velocity  $v_{\rm ref}=30~m/s$ . The initial conditions were set  $x(0)=0,\ v(0)=10,\ x_p(0)=300,\ v_p(0)=20,\ \rho_o^d(0)=20,\ \rho_o^d(0)=-40,\ \rho_o^d(0)=100,\ \rho_o^u(0)=-100,\ u(0)=0.$ 

Fig. 2(a) illustrates the evolution of the output tracking error  $e_o(t)$ , which remains strictly within the adaptive performance bounds  $\rho_o^d(t)$  and  $\rho_o^a(t)$ . Additionally, Fig. 2(b) depicts both the actual control input u(t) and the saturated control signal  $u_s(t)$ , as well as the control boundaries  $\bar{u}$ ,  $\underline{u}$ , showcasing the rate limiting ability of the proposed ACC scheme. It is worth noting that the actual control input u(t) is smoother than  $u_s(t)$ , avoiding the sharp accelerating peak observed at the first seconds of the simulation. The adaptive PFs adjusted effectively to dynamic driving conditions, ensuring that the tracking errors remained within the prescribed bounds. The ACC controller also addressed changes in the lead vehicle's speed, demonstrating its robustness in maintaining performance under versatile driving conditions. In Fig. 3(a), the vehicle's cruising velocity is shown. Initially, the vehicle accelerates to track the reference velocity, followed by a deceleration to maintain a safe distance from the leading vehicle. Thanks to the dynamic safety distance  $d_{b,r}(t)$ , which is illustrated in Fig. 3(b), the vehicle's deceleration is smooth and satisfies the constraints in (SC), (AC), (RC), and (OPC). Fig. 3(b) also shows the actual inter-vehicular distance d(t)compared with the minimum allowable distance  $\delta$ . Overall, the

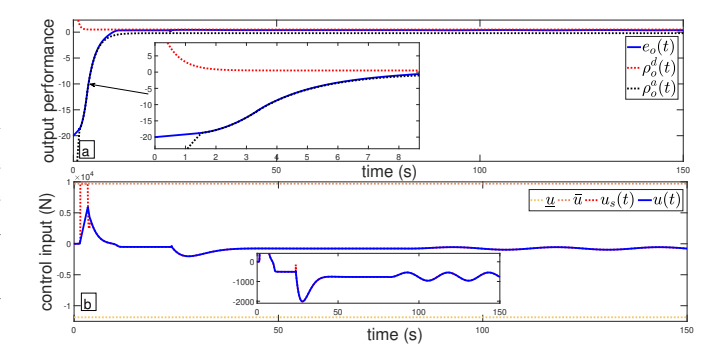


Fig. 2. (a): Adaptive performance bounds defined by the functions  $\rho_o^d(t)$  and  $\rho_o^a(t)$ , ensuring that  $e_o(t)$  remains strictly within the prescribed limits; (b): Actual control input u(t) compared with the saturated control signal  $u_s(t)$ , along with the input constraints  $\bar{u}=c_amg=9712~N$  and  $\underline{u}=-c_dmg=-11870~N$ .

ARC-ACC controller ensures safe and comfortable cruising along with adaptive performance specifications. The safety distance for braking  $d_{b,r}(t)$  is computed dynamically, ensuring robust safety margins throughout the simulation. Additionally, the adaptive PFs dynamically adjust the system's response to ensure the control input and its rate of change adheres to predefined saturation limits, effectively guaranteeing acceleration and jerk limits, ensuring passenger comfort as well. However, as observed in Fig. 3(b), the inter-vehicular distance at a cruising speed of 20 m/s is approximately 80 meters, which is somewhat conservative. This safety distance is directly influenced by the maximum deceleration rate, which is regulated by the parameter  $\underline{r} = -4000 \ N/s$ . This results in a maximum jerk of approximately  $3.6 m/s^3$  during deceleration, ensuring driver comfort even in the event of an abrupt stop by the preceding vehicle. To reduce the conservativeness of the safety distance, in the next simulation scenario, we select a lower r, closer to the mean deceleration rate observed in realworld emergency braking scenarios, thus achieving a more practical safety distance.

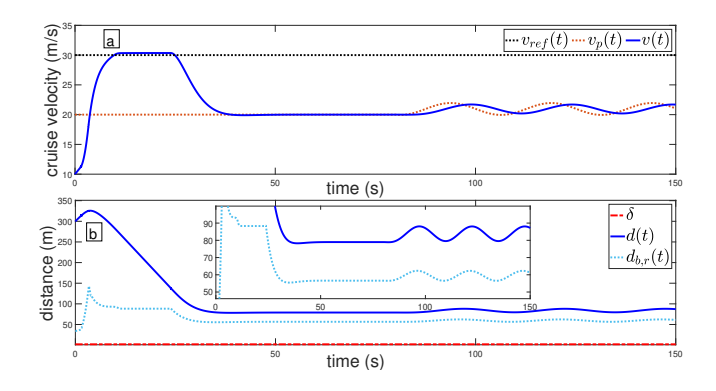


Fig. 3. (a): Evolution of the vehicle's cruising velocity; (b): Actual intervehicular distance d(t) along with the minimum allowable distance  $\delta$ , demonstrating compliance with safety distance requirements  $d_{b,r}(t)$ .

## B. Comparative Study

In this comparative simulation study, the performance of the proposed controllers AC-ACC and ARC-ACC was evaluated against the FCC introduced in [9], under identical driving conditions. The primary objective was to analyze their relative performance in terms of maintaining desired intervehicular distance, regulating vehicle speed, and respecting input constraints. The simulation scenario began with the lead vehicle cruising at a steady speed of 30 m/s, followed by an abrupt deceleration at 120 seconds until reaching 20 m/s, and subsequently accelerating at 150 seconds. The ACC controllers were configured to maintain a minimum intervehicular distance  $\delta = 2 m$  while tracking a reference velocity  $v_{\rm ref} = 40 \ m/s$ . The specific parameter settings for both AC-ACC and ARC-ACC are listed in Table I, except for the force and yank limits (rate of change of force), which were set to  $c_a = 0.8, c_d = 1, 1, \bar{r} = 1000 \ N/s, \underline{r} = -11000 \ N/s.$ Yank limits restrict the maximum jerk during deceleration to  $10 m/s^3$ , ensuring a balance between performance and passenger comfort. For fair comparison, the FCC scheme was structured similarly to the AC-ACC, with a proportional gain set to  $k = k_o = 45$ . The performance funnels were defined as:  $\phi_v(t) = (80 \exp{(-0.5t)} + 0.5)^{-1}$  and  $\phi_d(t) = (0.5)^{-1}$ . The initial conditions for the simulations were set as: x(0) = 0,  $v(0) = 5, x_p(0) = 500, v_p(0) = 40, \rho_o^d(0) = 0, \rho_o^a(0) = -80,$  $\rho_u^d(0) = 100, \; \rho_u^a(0) = -100, \; \text{and} \; u(0) = 0. \; \text{The safety}$ distance, considering the input constraints, was determined using (15) for the ARC-ACC and (5) for the AC-ACC and FCC.

Unlike the proposed controllers, which dynamically adjust the performance specifications in response to input constraints, the FCC does not explicitly account for these limitations. Instead, it relies on saturating the control signal outside a predefined compact set, which may lead to internal blowup of the controller, i.e., as the tracking error exceeds the performance boundary, the desired control signal diverges to infinity. To analyze this behavior, two scenarios were considered for the FCC, with limits set to  $c_a=0.8$  and  $c_a=0.9$ , respectively.

Fig. 4(a) illustrates the control signals generated by the different controllers. Notably, the control signal from the ARC-ACC is significantly smoother than those from the other controllers, effectively delimiting both acceleration and jerk during cruising. In contrast, the input generated by the AC-ACC and the FCC with  $c_a = 0.9$  are quite similar, except during the transient phase where the FCC exhibits a brief, sharp spike, generating a force of approximately 9700 N. In comparison, the AC-ACC generates a lower peak force of 8700 N. Figures. 4(b)-(c) illustrate the adaptive performance funnel for the ARC-ACC and AC-ACC schemes, while Figures 4(d)-(e) depict the predefined performance funnels for the FCC with  $c_a = 0.8$  and FCC with  $c_a = 0.9$  schemes, respectively. The FCC with  $c_a = 0.8$  suffers from internal blow-up, as the control effort is insufficient to keep the tracking error within the predefined performance funnel as shown in 4(d), ultimately leading to degraded performance.

Figures 5 and 6 present the actual inter-vehicular distance compared to the minimum allowable distance  $\delta$  and the ve-

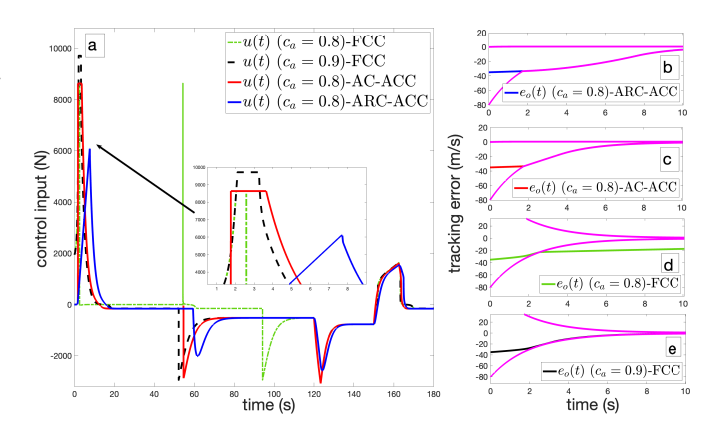


Fig. 4. (a): Control signals and (b)-(e): tracking errors along with the corresponding performance funnels generated by ARC-ACC, AC-ACC, and FCC.

hicle's cruising speed, respectively. While all schemes satisfy the safety distance constraint (SC) as shown in Fig. 5, the velocity tracking performance of the FCC with  $c_a=0.8$  exhibits degraded velocity tracking performance compared to the rest of the schemes, as depicted in Fig. 6. Notice that in the FCC with  $c_a=0.8$  the vehicle's velocity continues to increase until t=60 seconds, despite the control input being zero, due to the influence of gravity, as the road slope set at  $\theta=-0.1$  rad. Moreover, it can be seen from Fig. 5 that the inter-vehicle distance at cruising speed  $20 \ m/s$  is approximately  $45 \ \text{meters}$  compared to the  $80 \ \text{meters}$  of the previous simulation owing to the greater yank limit during decceleration.

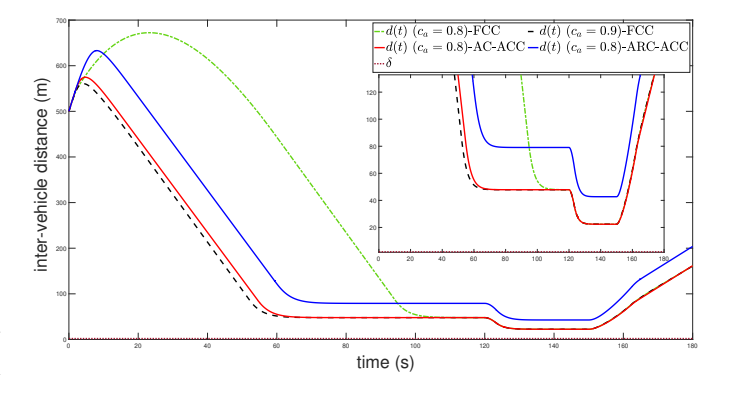


Fig. 5. Comparison of the actual inter-vehicular distance d(t) vs the minimum allowable distance  $\delta$  under the different ACC schemes.

## V. EXPERIMENTAL RESULTS

To validate the performance and the applicability of the proposed control scheme, an experimental procedure was conducted for the input-output constrained ACC problem using the ARC-ACC scheme. For the experiment we utilized two Husky A200 unmanned ground vehicles, as depicted in Fig. 7. In this setup, the lead vehicle was teleoperated to move in a straight line with a time-varying velocity, while the following vehicle implemented the ARC-ACC controller (16)-(28). To measure the inter-vehicular distance, the following vehicle was

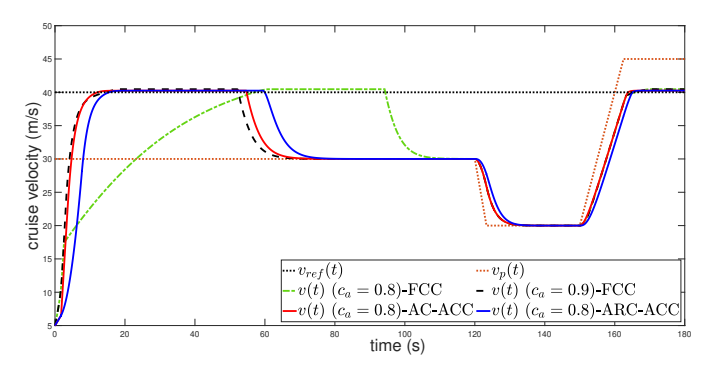


Fig. 6. Cruising speed comparison of the vehicle under the ACC schemes.

equipped with an Intel RealSense Depth Camera, and the lead vehicle was fitted with an ArUco marker to be detected by the camera.

The aim of the experiment is to demonstrate the controller's ability to incorporate multiple constraints and adapt soft constraints based on hard constraints, which represents the primary contribution of this work. In this vein, the control scheme was implemented at the kinematic level as described in Remark 6, where the control inputs were the desired velocities, since the embedded motor controller generated the necessary wheel torque to achieve these velocities precisely. As a result, the proposed controller in this ACC setup enforces both velocity and acceleration constraints on the vehicle. Based on the specifications of the Husky A200 robot, the maximum feasible speed is 1 m/s and the maximum acceleration is 3  $m/s^2$ . Accordingly, the control inputs were subject to saturation limits:  $\bar{u} = 0.9$ ,  $\underline{u} = 0$ ,  $\bar{r} = 3$ , and  $\underline{r} = -3$  ensuring that the generated control commands remain physically feasible for the robot. The control gains were defined as  $k_o = 0.045$ ,  $k_u = 0.3, c^w = 1, \gamma_o^j = 0.3 \text{ and } \gamma_u^j = 0.1 \text{ for } j = \{d, a\}.$ The minimum allowable distance was set at  $\delta = 1.99 \ m$ . The steady-state bounds for the PFs were set at  $\rho_o^{j,\infty} = 0.1$ and  $\rho_u^{j,\infty}=0.05$ , with the corresponding convergence rates chosen as  $\lambda_o^d=0.2$  and  $\lambda_o^a=2.5$  and  $\lambda_u^j=3$  for  $j = \{d, a\}$ . The control loop was executed with a time step of dt = 0.01 s, allowing for high-frequency updates and smooth, continuous control signals. The initial conditions were set as:  $x(0) = 0, \ v(0) = 0, \ x_p(0) = 3.49, \ v_p(0) = 0, \ \rho_o^d(0) = 0$ 0.1,  $\rho_o^a(0) = -2$ ,  $\rho_u^d(0) = 4$ ,  $\rho_u^a(0) = -4$ , u(0) = 0. The reference velocity was set to  $v_{ref}(t) = 0.8$  m/s, and the velocity-dependent safety distance  $d_{b,r}(t)$  was calculated based on (30). By applying the selected parameters  $\bar{u}$ ,  $\underline{r}$  and invoking (30) we determine that in the worst-case scenario, where the vehicle must decelerate from  $v(t) = \bar{u} = 0.9 \ m/s$ at the maximum deceleration rate  $\underline{r} = -3 \ m/s^2$ , the maximum traveled distance before stopping is  $\max(d_{b,r}) = 0.31 \ m$ . Thus, we incorporate this worst-case stopping distance into the reference inter-vehicular distance, which can be set as a fixed value:  $d_{\text{ref}} = \max(d_{b,r}) + \rho_o^{d,\infty} + \delta = 2.4 \text{ m.}$  The experiment demonstration can be accessed at: https://youtu. be/GKaBWztVO\_4.

The experimental results are presented in Fig. 8. In particular, Fig. 8(a) shows the actual inter-vehicular distance d(t),



Fig. 7. Experimental setup involving two Husky A200 unmanned ground vehicles.

which remains greater than the minimum allowable distance  $\delta$ , demonstrating collision avoidance throughout the experiment. Fig. 8(b) illustrates the evolution of the output tracking error  $e_o(t)$  along with its corresponding performance functions, while Fig. 8(c) presents the control tracking error  $e_u(t)$ , encapsulating the control deficiency owing to rate limitations.

The commanded velocity generated by the ACC controller is shown in Fig. 8(d), and the corresponding acceleration (i.e., the rate of change of the commanded velocity) is depicted in Fig. 8(e). The abrupt deceleration observed at t = 4 s results from the ACC scheme switching from velocity tracking to position tracking, triggered by the inter-vehicular distance approaching the safety threshold. When the relative distance increases again at  $t = 5 \,\mathrm{s}$ , the system resumes velocity tracking, resulting in re-acceleration. The velocity oscillations are primarily attributed to: (i) feedback delays introduced by the vision-based localization system (camera with ArUco markers), which degrade the accuracy of realtime state measurements, and (ii) the motion profile of the leading robot, which involves frequent starts and stops and generally moves at a lower speed than the follower's reference velocity (see https://youtu.be/GKaBWztVO\_4). These factors lead the controller to respond rapidly, producing fluctuations in the control signal.

The aforementioned oscillations could be mitigated through more exhaustive gain tuning, e.g., by reducing the value of  $c_o^w$ , which determines the influence of the distance error  $e_d(t)$  on the total output tracking error. Overall, the experimental results validate the effectiveness of the proposed controller in satisfying the constraints (SC), (AC), (RC), and (OPC), despite the presence of sensor inaccuracies and physical disturbances that are not present in computer simulations.

## VI. CONCLUSIONS

In this paper, we presented a robust ACC scheme that rigorously incorporates input, output and state constraints into the control strategy. The proposed scheme ensures the maintenance of a safe following distance, while the performance specifications are dynamically adjusted, to accommodate actuation limitations, including amplitude-and-rate input constraints. The simulation and experimental results validate the theoretical findings and showcase the effectiveness of

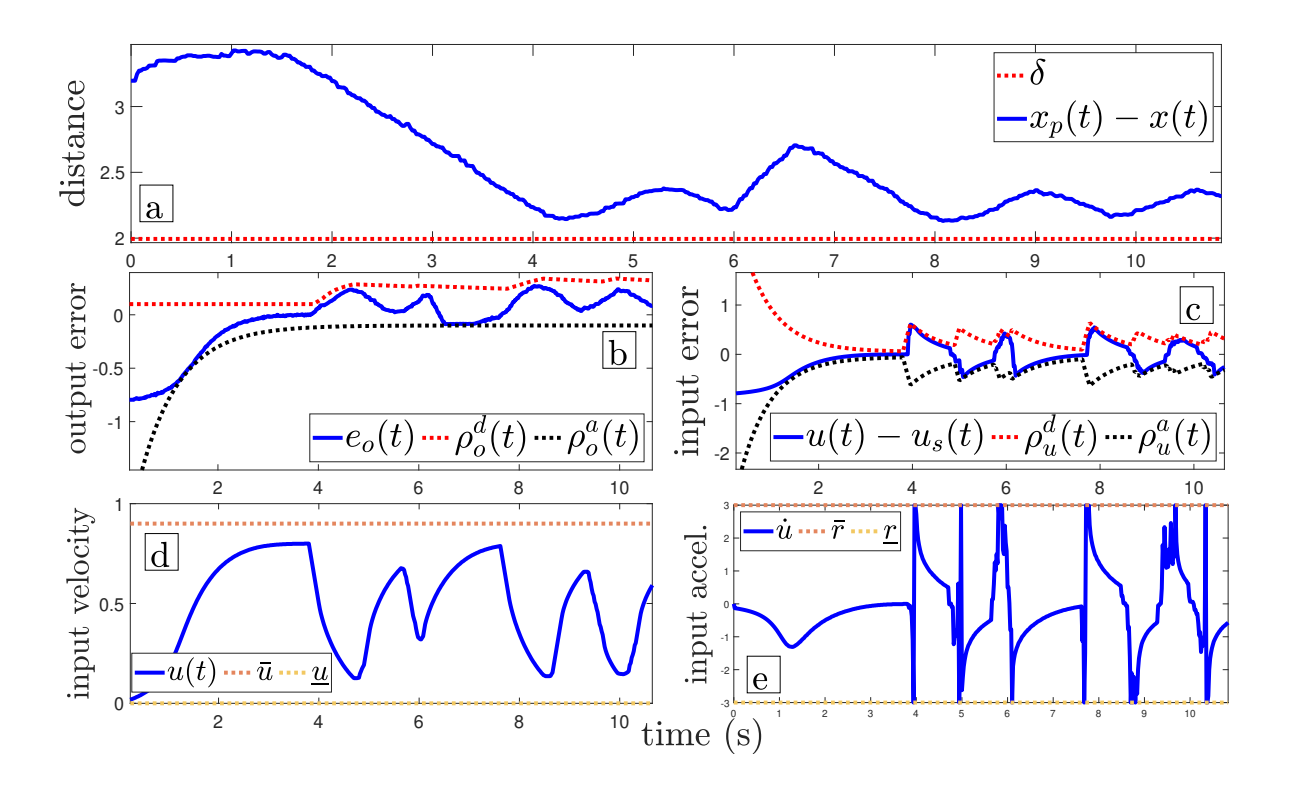


Fig. 8. Experimental results: (a) Actual inter-vehicular distance between d(t) vs the minimum allowable distance  $\delta$ ; (b) evolution of the output tracking error  $e_o(t)$  and its corresponding PFs; (c) evolution of the control tracking error  $e_u(t)$  along with the associated PFs; (d) commanded velocity generated by the ACC controller; (e) rate of change of the commanded velocity (acceleration) generated by the ACC controller.

the proposed controller, particularly in generating smooth control signals and ensuring robust performance across a wide range of driving scenarios, making it suitable for real-world autonomous driving applications. Since the proposed control framework does not incorporate any information about the preceding vehicle's dynamics, the safety distance which is updated online is conservative. As part of future work, we aim to reduce this conservativeness by incorporating vehicleto-vehicle communication and extending the ACC framework to handle multi-vehicle interactions in congested traffic conditions.

#### APPENDIX

*Proof of Theorem 1* Thenceforward, we omit the time argument for the closed-loop signals to enhance the clarity of the proof. Let us first define  $\psi \coloneqq \frac{e_d + \rho^a}{\rho^d - \rho^a}$  and recall that the output tracking error is  $e \coloneqq (1-w)e_v + c^w w e_d$  with time derivative given by:

$$\dot{e} = (1 - \dot{w})e_v + (1 - w)\dot{e}_v + c^w \dot{w}e_d + c^w w \dot{e}_d$$
 (31)

with:

$$\dot{e}_v = \frac{u + f_d(t, v)}{m} - \dot{v}_{ref}$$

$$\dot{e}_d = v - v_p + \dot{d}_{ref}$$
(32)

$$\dot{e}_d = v - v_p + \dot{d}_{ref} \tag{33}$$

$$\dot{w} = \begin{cases} 0 & \text{if } \psi < 0\\ \frac{\dot{e}_d + \dot{\rho}^a}{\rho^d - \rho^a} - \frac{(e_d + \rho^a)(\dot{\rho}^d - \dot{\rho}^a)}{(\rho^d - \rho^a)^2} & \text{otherwise} \end{cases}$$
(34)

Next, let the normalized error be written as  $\xi=\frac{e-\frac{1}{2}\tilde{\rho}_n}{\frac{1}{2}\tilde{\rho}_d}$ , with  $\tilde{\rho}_n := \rho^a + \rho^d$  and  $\tilde{\rho}_d := \rho^d - \rho^a$ . The time derivative of  $\xi$  is given by:

$$\dot{\xi} = \frac{2}{\tilde{\rho}_d} \left( \dot{e} - \frac{1}{2} \dot{\tilde{\rho}}_n - \frac{1}{2} \xi \dot{\tilde{\rho}}_d \right) 
= \frac{2}{\tilde{\rho}_d} \left( \dot{e} - \frac{1}{2} \left( \dot{\rho}^a (1 - \xi) + \dot{\rho}^d (\xi + 1) \right) \right).$$
(35)

Let the total state of the system described by (1) be denoted as  $s := [x, v]^T \in \mathbb{R}^2$ . Subsequently, we define the closed-loop system as follows:

$$\dot{\chi} \coloneqq \phi(t, \chi), \ \chi(0) \tag{36}$$

with  $\chi \coloneqq [s,\xi,\rho^a,\rho^d]^T$  denoting the state, which initializes within the open set  $\Omega_\chi \coloneqq \mathbb{R}^2 \times (-1,1) \times \mathbb{R}_{<0} \times \mathbb{R}_{>0}$ .

The proof proceeds through three phases. First, we establish the existence of a unique maximal solution to (36) over the time interval  $[0, \tau_{max})$ , ensuring that  $\chi(t) \in \Omega_{\chi}$  for all  $t \in [0, \tau_{max})$ . Next, we show that for every  $t \in [0, \tau_{max})$ , the proposed control strategy ensures that  $\chi$  remains strictly within a compact subset of  $\Omega_{\chi}$ . By contradiction, this implies that  $\tau_{max} = \infty$ , thereby guaranteeing the boundedness of all closed-loop signals for all t > 0.

Phase A: In the design procedure, we choose  $\rho^a(0)$  <  $e(0) < \rho^d(0)$ , which implies that  $\xi(0) \in (-1,1)$ , ensuring that the open set  $\Omega_{\chi}$  is non-empty. Moreover, the function  $\phi: \mathbb{R}_{>0} \times \Omega_\chi \to \mathbb{R}^5$  is locally Lipschitz with respect to  $\chi$  over the set  $\Omega_{\chi}$  and continuous with respect to t. Therefore, by applying Theorem 54 from [17] (pp. 476), we establish the existence and uniqueness of a maximal solution  $\chi:[0,\tau_{\max})\to\Omega_\chi$ , with  $\chi(t)\in\Omega_\chi$  for all  $t\in[0,\tau_{max})$  and  $\tau_{max}\in\{\mathbb{R}^*_{>0},\infty\}$ .

Phase B: It can be readily concluded that the model in (1) satisfies the input-to-state stability (ISS) property, as it is impossible to impose infinite velocity on a ground vehicle given bounded acceleration. Consequently, due to the input saturation, there exist a class  $\mathcal{K}$  function  $\gamma(\cdot)$  and a class  $\mathcal{KL}$  function  $\beta(\cdot,\cdot)$  such that  $s\in\Omega_s$ , where  $\Omega_s\coloneqq\{s\in\mathbb{R}^2:\|s(t)\|\leq\beta(\|s(0)\|,t)+\gamma(\|u\|_\infty)\}.$ 

Subsequently, note that the transformed error  $\epsilon(\xi)=\ln\left(\frac{1+\xi}{1-\xi}\right)$  lies in  $(-\infty,\infty)$  for  $\xi\in(-1,1)$  and consider the Lyapunov function candidate  $V:=\frac{1}{2}\epsilon^2$ . Differentiating V with respect to time and exploiting (11),(12),(35) we get:

$$\dot{V} = \zeta \epsilon (\dot{e} + \frac{1 - \xi}{2} \lambda^a (\rho^a + \mu \rho^{a,\infty}) 
+ \frac{\xi + 1}{2} \lambda^d (\rho^d - \mu \rho^{d,\infty}) - s_\gamma (u - u_d))$$
(37)

with  $s_{\gamma} \coloneqq \frac{s_{\gamma d}^e + s_{\gamma a}^{-e}}{2}$ . By differentiating (6) with respect to time and substituting the result into (33), we obtain:

$$\dot{e}_d = v \left( 1 - \frac{u + f_d(t, v)}{mg(c_d - \sin(\bar{\theta}))} \right) - v_p. \tag{38}$$

Note that the control input u is essentially bounded due to input saturation, which, by the ISS property of the system, implies the boundedness of v. Furthermore, by invoking Assumption 2, we can conclude that e is also bounded. Finally, considering the continuity of  $f_d(\cdot)$  and the fact that  $\dot{e}$  is a piece-wise continuous function of time involving bounded signals, there exists a positive constant H such that:

$$\left|\dot{e} + \frac{1-\xi}{2}\lambda^a(\rho^a + \mu\rho^{a,\infty}) + \frac{\xi+1}{2}\lambda^d(\rho^d - \mu\rho^{d,\infty}) - s_{\gamma}u\right| \le H$$

for any  $(\rho^a, \rho^d) \in \mathbb{R}_{<0} \times \mathbb{R}_{>0}$ . By letting  $\gamma = \frac{\max(\gamma^d, \gamma^a)}{2}$  and substituting (9) into (37) we arrive at:

$$\dot{V} \le H|\zeta\epsilon| - k\gamma|\zeta\epsilon|^2. \tag{39}$$

Notice that  $\dot{V} \leq 0$  when:

$$\left| \frac{\epsilon}{(\rho^d - \rho^a)(1 - \xi^2)} \right| \ge \frac{H}{k\gamma}. \tag{40}$$

It is important to note that the saturation effect on  $u_d$  does not occur when e=0. To proceed, we examine two distinct cases based on the sign of the tracking error e(t).

Case 1: When e>0 and the control signal  $u_d$  becomes saturated, the second term in (11) is activated, leading to an increase in the upper PF  $\rho^d$ , while the relaxation mechanism for  $\rho^a$  remains inactive. Let  $\rho^{a'}<0$  represent the value of  $\rho^a$  when the error e crosses zero into the right-half plane, which acts as a lower bound since (12) is strictly positive for all e>0. Exploiting (8) we have  $(\rho^d-\rho^a)(\xi+1)=2(e-\rho^a)$ . By multiplying (40) by  $|e-\rho^a|$  and substituting  $\epsilon(\xi)$ , we obtain:

$$\frac{\ln\left(\frac{1+\xi}{1-\xi}\right)(\xi+1)}{(1-\xi^2)} \ge \frac{2H|e-\rho^a|}{k\gamma}.\tag{41}$$

Note that the left-hand side of (41) is positive and increasing in  $|\xi|$ , while the right-hand side is upper bounded owing to the ISS property of (1) and the fact that  $\rho^a(t) \geq \rho^{a'}$ . Thus, there exists an  $\bar{\epsilon} := \epsilon(\bar{\xi}) > 0$  such that  $\dot{V} \leq 0$  for all  $\epsilon(t) \geq \bar{\epsilon}$ . It is obvious from (9) that the boundedness of  $\epsilon$  implies the boundedness of  $u_d(t)$ . Hence, let  $\bar{u}_d$  denote the upper bound of  $|u_d(t)|$  in the case where e>0, which corresponds to a braking scenario. Note that the actual control input u is essentially bounded because of input saturation. Moreover, by exploiting (11) we obtain:

$$\dot{\rho}^d \le -\lambda^d (\rho^d(t) - \rho^{d,\infty}) + \frac{\gamma \bar{u}_d}{(\xi' + 1)} \tag{42}$$

where  $\xi'$  is the smallest value of  $\xi(t)$ , at which the second term in equation (11) becomes active. Notice that the second term in (42) is bounded regardless of the amplitude of  $\rho^d(t)$ . Consequently, there exists  $\bar{\rho}^d>0$  for which  $\dot{\rho}^d\leq 0$ , and thus  $\rho^d(t)\leq \bar{\rho}^d$ , implying that  $\rho^d(t)\in [\mu\rho^{d,\infty},\bar{\rho}^d]\subset \mathbb{R}_{>0},\ \forall t\in [0,\tau_{\max}).$ 

Case 2: When e < 0 and the control signal  $u_d$  gets saturated, then the second term in (12) is activated and decreases the lower PF  $\rho^a$ , while the relaxation mechanism of  $\rho^d$  remains inactive. As in case 1, there exists an  $\underline{\epsilon} := \epsilon(\underline{\xi}) < 0$  such that  $\dot{V} \leq 0$  for all  $\epsilon(t) \leq \underline{\epsilon}$ . Let  $\underline{u}_d$  denote the upper bound of  $u_d(t)$  in case that e < 0, corresponding to an acceleration scenario. Similar to case 1, we obtain:

$$\dot{\rho}^a \ge -\lambda^a (\rho^a(t) + \mu \rho^{a,\infty}) - \frac{\gamma_{\underline{u}d}}{(1-\xi)} \tag{43}$$

Notice that the second term in (43) is bounded regardless of the amplitude of  $\rho^a(t)$ , while the first term is non-negative since  $\rho^a(t) \leq -\mu \rho^{a,\infty}$ . Consequently, there exists  $\bar{\rho}^a > 0$  for which  $\dot{\rho}^a \geq 0$ , and thus  $\rho^a(t) \geq -\bar{\rho}^a$ , leading to  $\rho^a(t) \in [-\bar{\rho}^a, -\mu \rho^{a,\infty}] \subset \mathbb{R}_{<0}, \ \forall t \in [0, \tau_{\max}).$ 

Phase 3: Based on the analysis above,  $\epsilon(t)$  is uniformly ultimately bounded with respect to the compact set  $\mathcal{E} := \{\epsilon : \underline{\epsilon} \leq \epsilon \leq \overline{\epsilon}\}$ . By denoting the inverse function of  $\epsilon(\xi)$  as  $T : \mathbb{R} \to (-1,1)$ , we obtain the following result:

$$-1 < T(\underline{\epsilon}) = \underline{\xi} \le \underline{\xi} \le \overline{\xi} = T(\overline{\epsilon}) < 1 \tag{44}$$

for all  $t\in[0,\tau_{\max})$ . As a result,  $\chi\in\Omega_s\times[\xi,\bar\xi]\times[-\bar\rho^a,-\mu\rho^{a,\infty}]\times[\mu\rho^{d,\infty},\bar\rho^d]\subset\Omega_\chi$  for all  $t\in[0,\tau_{\max})$ . According to Proposition C.3.6 from [17] (pp. 481), there should exist a time  $t'\in[0,\tau_{\max})$  where  $\chi(t')$  escapes  $\Omega_s\times[\xi,\bar\xi]\times[-\bar\rho^a,-\mu\rho^{a,\infty}]\times[\mu\rho^{d,\infty},\bar\rho^d]$  for all  $t\in[0,\tau_{\max})$ . However, this would contradict the assumption that  $\tau_{\max}<\infty$ . Hence, we conclude that  $\tau_{\max}=\infty$ . Moreover, since  $\xi(t)\in[\xi,\bar\xi]$  it follows that  $-\bar\rho^a\leq\rho^a(t)< e(t)<\rho^a(t)\leq\bar\rho^d$  ensuring that  $w(t)\in[0,1)$  for all  $t\geq0$ . Invoking the latter along with (7) we obtain:

$$\frac{\rho^a(t) - c^w w(t) e_d(t)}{1 - w(t)} < v(t) - v_{\text{ref}}(t) < \frac{\rho^d(t) - c^w w(t) e_d(t)}{1 - w(t)}$$

Note that during braking, i.e., e > 0 the performance function  $\rho^d$ , which serves as a barrier for e, increases only when maximum braking is applied, i.e., when the control signal  $u_d$  becomes saturated. In this scenario, the maximum traveled distance is given by (5). Once the saturation is no

longer active, the PF  $\rho^d$  retrieves its prescribed form with exponential rate, leading to a decrease in the tracking error e. This ensures that  $x_p(t) - x(t) > \delta$  for all  $t \geq 0$ , thus completing the proof.

<u>Proof of Corollary 1</u> First, consider the normalized errors  $\xi_o, \overline{\xi_u}$  as defined in Section III-B. The time derivatives of these errors are expressed as:

$$\dot{\xi}_{i} = \frac{2}{\tilde{\rho}_{d,i}} \left( \dot{e}_{i} - \frac{1}{2} \left( \dot{\rho}_{i}^{a} (1 - \xi) + \dot{\rho}_{i}^{d} (\xi + 1) \right) \right), \ i = \{o, u\}$$
(45)

with  $\tilde{\rho}_{d,i}(t) := \rho_i^d(t) - \rho_i^a(t)$ . Next, we define the extended closed-loop system as follows:

$$\dot{\eta} \coloneqq \kappa(t, \eta), \ \eta(0) \tag{46}$$

with  $\eta \coloneqq [s, \xi_o, \rho_o^a, \rho_o^d, \xi_u, \rho_u^a, \rho_u^d]^T$  denoting the state, which initializes within the open set  $\Omega_\eta \coloneqq \mathbb{R}^2 \times (-1, 1) \times \mathbb{R}_{<0} \times \mathbb{R}_{>0} \times (-1, 1) \times \mathbb{R}_{<0} \times \mathbb{R}_{>0}$ .

Subsequently, the proof proceeds through three phases, similar to the proof of Theorem 1. In fact, Phase 1 is identical to that of Theorem 1. Following the analysis from Phase 2 of Theorem 1, it is straightforward to show that s(t)remains within the compact set  $\Omega_s^{\eta} \coloneqq \{s \in \mathbb{R}^2 : ||s(t)|| \le 1\}$  $\beta(\|s(0)\|,t) + \gamma(\|u\|_{\infty})$ , where  $\gamma(\cdot)$  is a class K function and  $\beta(\cdot,\cdot)$  is a class  $\mathcal{KL}$  function, for all  $t \in [0,\tau_{\max})$ . Additionally, by recalling that  $\epsilon_o(\xi_o) = \ln\left(\frac{1+\xi_o}{1-\xi_o}\right)$  and introducing the positive definite function  $V_o \coloneqq \frac{1}{2}\epsilon_o^2$ , and following the analysis from Phase 2 of Theorem 1, as well as exploiting the boundedness of u(t) and  $u_s(t)$  owing to input saturation, we conclude that  $\epsilon_o$  is bounded with respect to a compact set  $\mathcal{X}_o := \{\xi_o : \xi_o \leq \xi_o \leq \overline{\xi_o}\} \subset (-1,1)$ , the size of which is influenced by the system dynamics and the reference signals. Furthermore, it is ensured that there exist constants  $\bar{\rho}_o^d > 0$  and  $\bar{\rho}_o^a < 0$  such that  $\rho^d(t) \in [\mu \rho^{d,\infty}, \bar{\rho}^d] \subset \mathbb{R}_{>0}$  and  $\rho^a(t) \in [\bar{\rho}^a, -\mu \rho^{a,\infty}] \subset \mathbb{R}_{<0} \text{ for all } t \in [0, \tau_{\max}).$ 

Next, consider the Lyapunov function candidate  $V_u := \frac{1}{2}\epsilon_u^2$ . Differentiating  $V_u$  with respect to time yields the following expression:

$$\dot{V}_{u} = \zeta_{u} \epsilon_{u} (\dot{e}_{u} + \frac{1 - \xi_{u}}{2} \lambda_{u}^{a} (\rho_{u}^{a} + \rho_{u}^{a,\infty}) 
+ \frac{\xi_{u} + 1}{2} \lambda_{u}^{d} (\rho_{u}^{d} - \rho_{u}^{d,\infty}) - s_{\gamma_{u}} (\dot{u} - u_{r})).$$
(47)

with  $s_{\gamma_u} \coloneqq \frac{s_{\gamma_u^d}^e + s_{\gamma_u^a}^{-e}}{2}$  and

$$\dot{e}_{u} = \operatorname{sat}_{\underline{r}}^{\overline{r}}(u_{r}) + k_{o} \frac{d}{du_{d}} \operatorname{sat}_{\underline{u}}^{\overline{u}}\left(u_{d}\right) \left(\dot{\zeta}_{o} \epsilon_{o} + \zeta_{o} \dot{\epsilon}_{o}\right).$$

Notice that  $\dot{u}$  is bounded due to the rate saturation. Moreover, the piece-wise continuous signal  $\dot{e}_u$  is bounded owing to the fact that  $\xi_o \in (-1,1)$  and the boundedness of  $\rho_o^d$  and  $\rho_o^a$ . Therefore, we conclude the existence of a positive constant  $H_u$  such that:

$$\left|\dot{e}_u + \rho_{\xi} - s_{\gamma_u} \dot{u}\right| \le H_u$$

with  $\rho_{\xi} \coloneqq \frac{1-\xi_u}{2} \lambda_u^a (\rho_u^a + \rho_u^{a,\infty}) + \frac{\xi_u+1}{2} \lambda_u^d (\rho_u^d - \rho_u^{d,\infty})$ , for any  $(\rho_u^a, \rho_u^d) \in \mathbb{R}_{<0} \times \mathbb{R}_{>0}$ . Substituting (25) into (47) we obtain:

$$\dot{V}_u \le H_u |\zeta_u \epsilon_u| - k_u |\zeta_u \epsilon_u|^2 \tag{48}$$

with 
$$\gamma_u = \frac{\max\left(\gamma_u^d, \gamma_u^a\right)}{2}$$
. Notably,  $\dot{V}_u \leq 0$  when:

$$\left| \frac{\epsilon_u}{(\rho_u^d - \rho_u^a)(1 - \xi_u^2)} \right| \ge \frac{H_u}{k_u \gamma_u}. \tag{49}$$

Furthermore, notice that  $e_u(t)$  is uniformly bounded with respect to a compact set  $[\underline{u}-\bar{u},\bar{u}-\underline{u}]$  owing to the amplitude saturation. Following the reasoning outlined in Phase 2 of Theorem 1, we conclude that  $\xi_u$  is uniformly bounded with respect to a compact set  $\mathcal{X}_u := \{\xi_u : \underline{\xi}_u \leq \xi_u \leq \bar{\xi}_u\}$ , with  $\bar{\xi}_u < 1$ . Additionally, there exist constants  $\bar{\rho}_u^d > 0$  and  $\bar{\rho}_u^a < 0$  such that  $\rho_u^d(t) \in [\rho_u^{d,\infty},\bar{\rho}_u^d] \subset \mathbb{R}_{>0}$  and  $\rho_u^a(t) \in [\bar{\rho}_u^a,-\rho^{a,\infty}] \subset \mathbb{R}_{<0}$  for all  $t \in [0,\tau_{\max})$ . Consequently, for all  $t \in [0,\tau_{\max})$ ,  $\eta$  belongs to the compact set  $\Omega_s^\eta \times \mathcal{X}_o \times [\bar{\rho}_o^a,-\mu\rho_o^{a,\infty}] \times [\mu\rho_o^{d,\infty},\bar{\rho}_o^d] \times \mathcal{X}_u \times [\bar{\rho}_u^a,-\rho_u^{a,\infty}] \times [\rho_u^{d,\infty},\bar{\rho}_u^d]$  which is clearly a subset of the open set  $\Omega_\eta$ . This inclusion, combined with the analysis presented in Phase 3 of Theorem 1 ensures that all closed-loop signals are UUB as well as that  $\rho_o^a(t) < e(t) < \rho_o^d(t)$  for all  $t \geq 0$ .

Subsequently, we have to determine the safety distance considering the worst-case scenario where the vehicle must brake at maximum capacity  $-c_d mg$ , in presence of constraints regarding the rate of change in the control input. In this extreme scenario, the desired rate of change (25) of the control signal u saturates and the vehicle has to decelerate at full negative rate  $\underline{r}$ . First, we calculate the distance required until the control input u(t) reaches the maximum braking force,  $\underline{u} = -c_d mg$ , assuming that u(t) decreases linearly at the maximum negative rate  $\underline{r}$ . In particular:

$$u(t+\tau) = u(t) - |r|\tau. \tag{50}$$

Solving (50) for  $t_r$  seconds ahead, when  $u(t + t_r) = -c_d g m$  we get:

$$t_r = \frac{u(t) + c_d gm}{|\underline{r}|}. (51)$$

Leveraging (2) and (50) the velocity during deceleration is given by:

$$v(t+\tau) = v(t) + \frac{1}{m} \int_{0}^{\tau} u(t) - |\underline{r}|\tau' - mg\sin(\theta(t+\tau))d\tau'$$
$$\leq v(t) + \frac{(u(t) + mg\sin(\bar{\theta}))\tau - \frac{|\underline{r}|}{2}\tau^{2}}{m}$$

Therefore, the worst-case travelled distance after  $t_r$  seconds, is:

$$x(t+t_r) = x(t) + \int_{0}^{t_r} v(t+\tau)d\tau = x(t) + d_b^r(t)$$

with.

$$d_b^r(t) := \frac{(u(t) + mg\sin(\bar{\theta}))t_r^2}{2m} + v(t)t_r - \frac{|\underline{r}|t_r^3}{6m}.$$
 (52)

The adaptive performance bound, governed by (27), expands until the first term in (27) dominates. Once the saturation effect in (25) becomes inactive, the rate of change in u(t) is dictated solely by  $\dot{\rho}_u^d = -\lambda_u^d(\rho_u^d(t) - \rho_u^{d,\infty})$ . Consequently, the vehicle decelerates at the maximum negative rate until a time instant

 $t' < t_r$ . As a result, there exists a time instant t'' such that  $|\dot{u}(t)| < |\underline{r}|$  for all  $t \in [t',t_r+t'']$ , where  $t_r+t''$  is the time when  $u = -c_d mg$ . During this time interval,  $u_r$  does not saturate, and the rate of convergence of the error  $e_u$  is at least  $\exp{(-\lambda_u^d t)}$  for all  $t \in [t',t_r+t'']$ . As a result, the minimum deceleration rate, denoted by  $l(\lambda_u^d)$ , is increasing in  $\lambda_u^d$ . Next, we show that for appropriately chosen values of  $\lambda_u^d$ , the distance traveled up to  $t_b^r = t + t_r + t''$  remains less than  $d_b^r(t)$ , ensuring that the safety inter-vehicular distance is maintained. Specifically, invoking (52), we aim to satisfy the condition:

$$v_2(t) - \frac{l(\lambda_u^d)t_2^3}{6m} \le v_1(t) - \frac{|\underline{r}|t_1^3}{6m} =: \beta_r$$
 (53)

where:

$$\begin{split} v_1(t) &\coloneqq \frac{(u(t+t') + mg\sin{(\bar{\theta})})t_1^2}{2m} + v(t+t')t_1, \\ v_2(t) &\coloneqq \frac{(u(t+t') + mg\sin{(\bar{\theta})})t_2^2}{2m} + v(t+t')t_2, \end{split}$$

with  $t_1 = t_r - t'$  and  $t_2 = t_1 + t''$ . After straightforward algebraic manipulations, inequality (53) becomes:

$$l_u^* := l(\lambda_u^d) \ge \frac{6m(\upsilon_2(t) - \beta_r)}{t_2^3}.$$
 (54)

Finally, by combining (5) and (52) and omitting the last term of (52), in order to facilitate the selection of  $l_u^*$ , we define the safety distance as:

$$d_{b,r}(t) := \frac{v(t)^2}{2g(c_d - \sin(\bar{\theta}))} + \frac{(u(t) + mg\sin(\bar{\theta}))t_r^2}{2m} + v(t)t_r$$

with  $t_r=\frac{u(t)+c_d mg}{|r|}$ , for which the proposed scheme (16)-(28) guarantees that for any  $\lambda_u^d \geq l^{-1}(l_u^*)=:\lambda_u^*$ , the inter-vehicular distance satisfies  $d(t)>\delta$ , thereby completing the proof.

## REFERENCES

- [1] C. Rödel, S. Stadler, A. Meschtscherjakov, and M. Tscheligi, "Towards autonomous cars: The effect of autonomy levels on acceptance and user experience," in *Proceedings of the 6th International Conference* on Automotive User Interfaces and Interactive Vehicular Applications. New York, NY, USA: Association for Computing Machinery, 2014, pp. 1–8.
- [2] C. C. Chien and P. Ioannou, "Automatic vehicle-following," in 1992 American Control Conference, 1992, pp. 1748–1752.
- [3] D. Yanakiev and I. Kanellakopoulos, "Nonlinear spacing policies for automated heavy-duty vehicles," *IEEE Transactions on Vehicular Tech*nology, vol. 47, no. 4, pp. 1365–1377, 1998.
- [4] B. van Arem, C. J. G. van Driel, and R. Visser, "The impact of cooperative adaptive cruise control on traffic-flow characteristics," *IEEE Transactions on Intelligent Transportation Systems*, vol. 7, no. 4, pp. 429–436, 2006.
- [5] G. Gunter, D. Gloudemans, R. E. Stern, S. McQuade, R. Bhadani, M. Bunting, M. L. Delle Monache, R. Lysecky, B. Seibold, J. Sprinkle, B. Piccoli, and D. B. Work, "Are commercially implemented adaptive cruise control systems string stable?" *IEEE Transactions on Intelligent Transportation Systems*, vol. 22, no. 11, pp. 6992–7003, 2021.
- [6] K. Santhanakrishnan and R. Rajamani, "On spacing policies for highway vehicle automation," *IEEE Transactions on Intelligent Transportation Systems*, vol. 4, no. 4, pp. 198–204, 2003.
- [7] A. D. Ames, J. W. Grizzle, and P. Tabuada, "Control barrier function based quadratic programs with application to adaptive cruise control," in 53rd IEEE Conference on Decision and Control, 2014, pp. 6271–6278.
- [8] A. D. Ames, X. Xu, J. W. Grizzle, and P. Tabuada, "Control barrier function based quadratic programs for safety critical systems," *IEEE Transactions on Automatic Control*, vol. 62, no. 8, pp. 3861–3876, 2017.

- [9] T. Berger and A.-L. Rauert, "Funnel cruise control," Automatica, vol. 119, no. 109061, 2020.
- [10] P. S. Trakas and C. P. Bechlioulis, "Adaptive performance control for input constrained MIMO nonlinear systems," *IEEE Transactions on Systems, Man, and Cybernetics: Systems*, vol. 54, no. 12, pp. 7733– 7745, 2024.
- [11] P. S. Trakas and C. P. Bechlioulis, "Robust adaptive prescribed performance control for unknown nonlinear systems with input amplitude and rate constraints," *IEEE Control Systems Letters*, vol. 7, pp. 1801–1806, 2023
- [12] K. J. Åström and R. Murray, Feedback systems: an introduction for scientists and engineers. Princeton university press, 2021.
- [13] B. L. Boada, M. J. L. Boada, and H. Zhang, "Sensor fusion based on a dual kalman filter for estimation of road irregularities and vehicle mass under static and dynamic conditions," *IEEE/ASME Transactions* on *Mechatronics*, vol. 24, no. 3, pp. 1075–1086, 2019.
- [14] C. P. Bechlioulis and G. A. Rovithakis, "Robust adaptive control of feedback linearizable MIMO nonlinear systems with prescribed performance," *IEEE Transactions on Automatic Control*, vol. 53, no. 9, pp. 2090–2099, 2008.
- [15] F. Mehdifar, C. P. Bechlioulis, and D. V. Dimarogonas, "Funnel control under hard and soft output constraints," in 2022 IEEE 61st Conference on Decision and Control (CDC), 2022, pp. 4473–4478.
- [16] P. S. Trakas and C. P. Bechlioulis, "Approximation-free adaptive prescribed performance control for unknown SISO nonlinear systems with input saturation," in 2022 IEEE 61st Conference on Decision and Control (CDC), 2022, pp. 4351–4356.
- [17] E. D. Sontag, Mathematical Control Theory: Deterministic Finite Dimensional Systems (2nd Ed.). Berlin, Heidelberg: Springer-Verlag, 1998.



Panagiotis S. Trakas (Student Member, IEEE) was born in Tripoli, Greece, in 1998. He received the Diploma in Electrical and Computer Engineering from the Aristotle University of Thessaloniki, Thessaloniki, Greece, in 2021. He is currently pursuing the Ph.D. degree in Electrical and Computer Engineering at the University of Patras, Patras, Greece.

Between 2023 and 2024, he was a Visiting Scholar at the Division of Signals and Systems, Uppsala University, Uppsala, Sweden, and the Robot Perception and Learning (RPL) Lab at the University College

London (UCL), London, U.K. His research interests include nonlinear robust adaptive control, control of robotic vehicles, and multiagent systems.



Valerio Modugno (Member, IEEE) received the Ph.D. degree from the Sapienza University of Rome, in 2017. He was a Visiting Researcher at the Technical University of Darmstadt, in 2014, and the INRIA Grand-Est Nancy, in 2015. He was a Post-doctoral Researcher for four years at the Sapienza University of Rome, under the supervision of Profa Giuseppe Oriolo. He joined University College London (UCL), in 2022, where he worked as a Research Fellow with the RPL Laboratory. Since 2024, he has been an associate lecturer at UCL with the robotics

group. His research interests include comprise humanoid whole-body control, optimal control, teleoperation for legged robots, reinforcement learning, black-box optimization, and safety for control and learning strategies.



Dimitrios Kanoulas (Member, IEEE) received the Ph.D. degree in computer science from Northeastern University, Boston, MA, USA. He is currently a Professor in Robotics and AI with the Department of Computer Science, University College London, and a UKRI Future Leaders Fellow. He was a Post-doctoral Researcher at the Italian Institute of Technology for five years. He has authored or coauthored more than 90 research papers in high-impact journals and conferences. His research interests include robot perception, planning, and learning.



Charalampos P. Bechlioulis (Senior Member, IEEE) was born in Arta, Greece, in 1983. He is currently an Associate Professor with the Division of Systems and Control, Department of Electrical and Computer Engineering, University of Patras. He received a diploma in electrical and computer engineering in 2006 (first in his class), a bachelor of science in mathematics in 2011 (second in his class) and a Ph.D. in electrical and computer engineering in 2011, all from the Aristotle University of Thessaloniki, Thessaloniki, Greece. His research interests

include nonlinear control with prescribed performance, system identification, control of robotic vehicles and multi-agent systems. He has authored more than 140 papers in scientific journals and conference proceedings and 3 book chapters.